Monte Carlo simulations of spectral albedo for artificial snowpacks composed of spherical and non-spherical particles

By

Tomonori Tanikawa
Department of Civil Engineering, Kitami Institute of Technology, Koencho 165, Kitami, Hokkaido 090-8507, Japan.

Teruo Aoki
Department of Physical Meteorology Research, Meteorological Research Institute, 1-1, Nagamine, Tsukuba, Ibaraki-ken 305-0052, Japan.

Masahiro Hori
Earth Observation Research Center, Japan Aerospace Exploration Agency, Harumi Island Triton Square Office Tower X 23F, 1-8-10, Harumi, Chuo-ku, Tokyo 104-6023, Japan.

Akihiro Hachikubo
New Energy Resources Research Center, Kitami Institute of Technology, Koencho 165, Kitami, Hokkaido 090-8507, Japan.

Osamu Abe
Shinjo Branch of Snow and Ice Studies, National Research Institute for Earth Science and Disaster Prevention, Takadan 1400, Tokamachi, Shinjo, Yamagata-ken 996-0091, Japan.

and

Masamu Aniya
Graduate School of Life and Environmental Sciences, University of Tsukuba, 1-1-1, Tennoudai, Tsukuba, Ibaraki-ken 305-8572, Japan.

Published by Applied Optics 2006

Abstract

The optical properties of snowpacks composed of spherical and non-spherical particles artificially prepared in a cold laboratory are investigated by measuring spectral albedos. The measured spectral albedo in the spectral region λ = 0.35 to 2.5 μm is compared with the theoretically calculated albedo, for which a Monte Carlo radiative transfer model is employed for multiple scattering combined with the Mie theory and the ray-tracing technique for single scattering by snow particles. Since the spherical particles are a little aggregate, the effects of cluster of the spheres on snow albedo are examined using a generalized multiparticle Mie-solution model (Xu, 1995, 2003). The snow albedo of cluster of the spheres can be represented with that of the singe sphere slightly larger than its component of the cluster in case of small grains. The observed albedos for the spherical snow particles agree with the theoretically calculated ones for the snow grain size measured in the snow pit work. The snow albedos for the non-spherical particles, which were dendrites, are influenced by the branch width and the branch length, based on a comparison of the theoretically calculated albedo using circular cylindrical snow particles and the observed albedo. The snow albedo in the near-infrared region depends on the branch width only when the branch length is sufficiently greater than the branch width. The comparison between the spherical and non-spherical snow particles indicates that the spectral albedo of the non-spherical particles can be represented using an equal volume/area ratio sphere.

1. Introduction

Changes in snow-covered areas have been studied in relation to global climate changes and water cycles. Results of monitoring the snow cover extent by satellite data indicate that it has decreased by about 10 % in the northern hemisphere since 1966.[1] The temperature trend is related to changes in the snow cover, since the snow influences the surface temperature.[2] Thus, the presence of snow strongly affects the Earth's snow melting and heat budget.

Snow albedo is also an important factor that affects the Earth's snow melting and heat budget. The snow albedo is generally high and plays a role in protecting against absorption of shortwave radiation entering the snow surface. However, the snow albedo depends on the snow condition and/or the seasonal variation and controls the melting rate.[3,4] Moreover, the atmospheric exhaust of the aerosols from human activities decreases the snow albedo.[5,6] It is necessary to accurately estimate the snow albedo since the albedo is an important boundary condition, not only for predicting seasonal snowmelt and runoff rates but also for understanding the extent and/or retreat of snow-covered areas.[7]

Various studies have focused on measuring of snow albedo. Liljequist[8] measured the albedo in four spectral bands in clean Antarctic snow. His analysis has been a pioneering work to subsequent radiation measurements. Measurements of albedo with high spectral resolution have been reported, and the effects of the snow physical parameters on the spectral albedo of the snow lifetime from new snow to granular snow have been investigated.[9-12] From the measurements of spectral snow albedo, the optical equivalent snow grain size is in the order of the branch width of dendrites of new snow.[13,14] The relationship between the change in size distribution of the snow grains and the spectral albedo was examined by controlling the snow metamorphism in a cold laboratory.[15] This examination indicated that increasing the snow grain size leads to broadening of the snow grain size distribution and a resultant reduction of the spectral albedo. Aoki *et al.*[4] conducted radiation budget observations simultaneously with snow pit work during two winters in Hokkaido, Japan, and reported that dependence of the snow albedo on the elapsed time after snowfall could be clearly classified by dividing the snow-covered period into a dry season and a wet snow season rather than by snow surface temperature.[4]

A radiative transfer model of snow was developed to demonstrate the significant effects of the snow physical parameters on the spectral albedo and to predict the snow albedo in the land-surface models used in general circulation models (GCMs). Wiscombe and Warren[16] examined the effects of the solar zenith angle, snow grain size, impurities, and snowpack thickness on the spectral snow albedo using the radiative transfer model of snow. The effect of impurities contaminating the snow on the spectral albedo has been also examined.[17,18] It is possible to use the radiative transfer model of the snow-atmospheric system to retrieve the snow albedo and physical parameters using the airborne and satellite data.[19-23] Inputting results of analyzed remote-sensing data to the land-surface model enables accurate predictions of the global climate changes.

These radiative transfer models of snow have addressed many problems, but they were not designed to clarify the microstructure of snow grain. Most radiative transfer models are based on the assumption of spherically shaped snow grains.[13,14,16] However, snow crystals have a complex structure and consist of irregularly shaped ice grains in contact with other grains, and the single-scattering properties differ between spherical and non-spherical particles.[24, 25] The spherical particle model has limited applicability to snow optics.[26] Therefore, optical measurements of snow are necessary to examine the optical properties of non-spherical particles to accurately calculate snow albedo.

The purpose of this study is to investigate the optical properties of spherical and non-spherical ice particles using spectral albedo data, snow pit work data, and the radiative transfer model. We performed the measurements of snow albedo for different artificial snow types produced in a cold laboratory under constant illumination conditions. The theoretically calculated spectral albedos obtained using the ray-tracing technique for single scattering and a Monte Carlo radiative transfer model for multiple scattering, taking into account the instrument setup in the cold laboratory, were compared with the measured results for two types of artificial snow.

2. Experiment

A. Cold laboratory

Spectral snow albedo measurements and snow pit work were carried out in a cold laboratory in the Shinjo Branch of Snow and Ice Research Group, National Research Institute for Earth Science and Disaster Prevention, Japan (http://www.bosai.go.jp/seppyo/mokuji/mokuji_framepage_e.htm). The snow used for our experiment was snow cover artificially produced from fresh artificial snowfall of spherical particles and half-sized dendrites. The process of making the artificial snow is as follows: the water and compressed air are emitted mistily by nozzle in cooling-air of -15C° or less, and then ice crystal are formed with the adiabatic expansion of air and put on a plastic belt just below the ceiling of the cold laboratory. Finally the artificial snow grows into semi-symmetrical dendrites shapes that are incomplete since they were artificially grown on the plastic belt.[15] The instrument setup is shown in Fig. 1. The snow accumulated in a container of 3 m by 5 m in size with a wall height of 0.2 m. The light source consisted of 739 metal halide lamps mounted on a 3.2 m by 5.7 m plate above the snow container. The lamps were directed for the emitted angle of the light (Fig. 2), and thus the light incident upon the snow surface was not parallel, and the snow surface was illuminated somewhat diffusely. Results of the measured spectral directivity indicated almost no dependence of directivity on the wavelength. We used a light power of 300 Wm^{-2} located 3.3 m above the snow surface, which did not melt the snow during the experiment. The air temperature in the cold laboratory was kept at about -20 °C. Details of the artificial snow and instruments in the cold laboratory are described in Ref. 15.

B. Snow condition

Two types of snow were prepared for this experiment, spherical particles (hereafter, case S) and dendrites (hereafter, case D). Figure 3 shows micrographs of artificial snow crystals. The cluster of grains in case S consisted of spherical particles that bonded with each other; however snow grain was not more aggregative than that in the micrographs when we made an optical measurement. The snow depths for case S and case D were 31 cm and 57 cm, respectively as indicated in Fig. 4. The snowpack of dendrites in case D was spread over the layer of spherical particles, since the snow density of dendrites is very small and the optical depth may be insufficient for a snow depth of only 31.5 cm. The snow grain size (radius) was measured at a 10 μm resolution using a handheld lens and the same method as that used by Aoki *et al.*[13] Two grain size dimensions were measured during this experiment. The first dimension was one-half the length of the major axis of the dendrites or cluster of aggregated grains (r_1) while the second dimension was one-half the branch width of the dendrites or each spherical particle (r_2). The snow grain sizes r_1 and r_2 in the layer from the surface to 5 cm for case S were less than 100 μm and 10 to 30 μm, respectively, and those below 5 cm deep were less than 100 μm and 20 to 40 μm, respectively. There were two snow layers for case S because the snow surface was rough just after snowfall and we artificially smoothed it. The upper layer of case D (0 to 31.5 cm) consisted of snow grains of $r_1 < 500$ μm and $r_2 = 10$ to 30 μm, and the lower layer (31.5 to 57 cm) was similar to that for case S. The snow density of the spherical particles was one order of magnitude greater than that of the dendrites. The temperatures of the two types of snow were all below the freezing point and were nearly constant at around -16 °C. There was no contamination in the snow.

C. Instrumentation and spectral data

The downward and upward (snow-reflected) components of the radiant flux densities were spectrally measured with a grating-type spectrometer, "FieldSpec FR," made by ASD Inc. (USA). The scanning spectral range of this instrument is $\lambda = 0.35$ to 2.5 μm, with a spectral resolution of 3 nm for $\lambda = 0.35$ to 1.0 μm and 10 nm for $\lambda = 1.0$ to 2.5 μm. We used a white reference standard (WRS) of spectralon made by Labsphere Inc. (USA) to observe the spectral albedo, as shown in Fig. 1. The upward and downward fluxes were obtained by measuring the reflected lights from the upper and lower sides of the WRS with the optical fiber tip of the spectrometer. The spectral albedo was calculated by averaging five measurements. The WRS (6 × 6 cm) was kept at a height of 10 cm above the snow surface and fixed 1 m from the side of the snow container (Fig. 1). We believe that the effect of the WRS's shadow over the snow surface on the observed albedo cannot be ignored with the WRS in such a low position. The optical measurements in the cold laboratory differed somewhat from the field measurements in that the snow area was finite, some photons escaped from the snow wall (Fig. 1), the light source area was finite, and the emitted light was not parallel. We therefore must consider these effects of the instrument setup on the simulated albedos.

3. Radiative transfer model

We used a radiative transfer model (RTM) based on the Monte Carlo method (MC-RTM) (e.g. Marchuk *et al.*[27]) to simulate the spectral snow albedo for the finite illumination conditions in a cold laboratory. Three key steps are necessary to simulate the experiment with the Monte Carlo method, i.e., generation of the photons based on lamp directivity (Fig. 2), localization of the

photon-object intersection, and determination of the type of interaction (scattering or absorption) and the scattering direction. Each snow layer in this model, shown in Fig. 4, was assumed to be optically homogeneous.

For single scattering properties (single scattering albedo, phase function, and extinction efficient), we used the conventional light scattering theories, Mie theory, for case S and the ray-tracing technique[28] for case D, based on the far-field approximation. In the conventional light scattering theories, the scattering pattern is obtained for a single particle in isolation; however, we show in many literatures that the models agree quite well with measured spectral albedo even for densely packed snow (e.g. Ref. 14, 16, 29, and 30), although the asymmetry parameters for densely packed grain are smaller than those for independently scattering sphere.[31-33] This is because at visible and near-infrared regions the grain sizes and spaces between grains are very large compared with the wavelength of light, so the approximation of independent scattering may be used in practical computations for densely packed media (e.g. Ref. 16, 29, 31, and 33). This means that the effect of the densely packed medium on the snow albedo does not influence the behavior of the snow albedo fundamentally. We applied the conventional light scattering theory to the snow albedo calculations.

On the other hand, small particle often have an aggregate structure of complex morphology in nature. In Fig. 3a, snow grains are aggregates composed several or more smaller spherical particles; however, in truth, snow grain was not more aggregative than that in the micrographs when we made an optical measurement just after the snowfall. We examined the effect of cluster of the spheres on the snow albedo using a generalized multiparticle Mie-solution model.[34, 35] Since this code is time-consuming when particle number and/or particle size become large, we made the comparison under the following conditions. The size of the single sphere used r = 10 μm for λ = 0.55 μm and r = 15 μm for λ = 2.2 μm, respectively. For the cluster of spheres, we checked the micrographs again and set a cluster of three identical spheres for λ = 0.55 μm. This is because the effect of aggregation on the single scattering is very small due to the weak absorption of ice.[36] For λ = 2.2 μm, the cluster of three, five and ten identical spheres was set, respectively. For configurations of the cluster, asymmetric and symmetric clusters are used. The volume equivalent grain size is r_V = 14.4, 25.6 and 32.3 μm for the cluster of three, five and ten spheres, respectively.

The asymmetry factors of the cluster of the spheres are somewhat smaller than those of the single sphere, even though the cluster of the spheres is bigger than the single sphere. The single scattering albedo of the cluster of the spheres is approximately equal to that of the single sphere at λ = 0.55 μm, while the single scattering albedo decreases with increasing the number of spheres at λ = 2.2 μm: $\tilde{\omega}_S = 0.977$, $\tilde{\omega}_{C3} = 0.974$, $\tilde{\omega}_{C5} = 0.972$ and $\tilde{\omega}_{C10} = 0.961$ for the single sphere, the cluster of three, five and ten identical spheres, respectively. The comparison between the albedo of the cluster of the spheres α_C and the single sphere α_S was made at solar zenith angle of 50°, which is an effective zenith angle for purely diffuse radiation.[16] The relative errors between both albedos $(\alpha_S - \alpha_C)/\alpha_S \times 100$ are 0.03 % at λ = 0.55 μm, and 1.43 %, 2.70 % and 14.36 % for the cluster of three, five and ten spheres at λ = 2.2 μm. We agreed with the study of Mishchenko *et al*.[37] in which the most important factor in light scattering by a few component cluster would be the shape of the component particles from the study of light scattering properties of the simplest aggregated particles. From these comparisons, the snow albedo of the cluster of the spheres can be represented with that of the singe sphere slightly larger than its component of the cluster in case of small grains.

For the snow albedo calculation, the complex refractive indices of ice were taken from

Warren[38] for $0.35 \leq \lambda \leq 1.4$ μm and Kou *et al.*[39] for $\lambda \geq 1.45$ μm. The snow albedos are calculated for eleven wavelengths (λ = 0.35, 0.55, 0.675, 0.875, 1.05, 1.25, 1.5, 1.65, 1.85, 2.0 and 2.2 μm). These wavelengths, except for λ = 1.5, 1.85, and 2.0 μm, were the atmospheric windows used in the airborne (e.g. Ref. 20, 22, 23) and satellite remote sensing (e.g. Ref. 40-42) for the mass concentration of snow impurities and the snow grain size.

4. Results and discussion

A. Observed spectral snow albedo

Figure 5 presents the observed spectral albedos for case S and D. The spectral albedos at the visible wavelengths were relatively lower than those of natural pure snow (albedo $\alpha > 0.95$ at λ = 0.55 μm), despite there being no snow impurities contaminating our artificial snow. The theoretically calculated albedos for r_{eff} = 10, 20, and 50 μm using doubling and adding RTM (DA-RTM) for plane-parallel snow[14] are also indicated in Fig. 5 as a comparison of the theoretical albedo of pure snow with the observed albedo for case S. This model assumes a snow layer 31 cm depth with a snow density of 0.155 g/cm^3, which were determined in the snow pit work (Fig. 4a). The theoretically calculated spectral albedo for r_{eff} = 20 μm agreed well with the observed one in the region of $\lambda \geq 1.4$ μm; however, for $\lambda < 1.4$ μm, the theoretically calculated albedos for any value of r_{eff} exceeded the observed ones. This is explained by the characteristics of the instrument setup in the cold laboratory, i.e., the effects of a finite snowfield and the snow wall, the effects of a finite light source, and the height of the WRS. Details of these effects on the spectral albedo are described in Appendix A.

In the Fig. 5, there was a few difference of albedo between case S and D in the near-infrared regions, while little difference of that in the visible regions due to weak light absorption. Since the near-infrared snow-albedo is sensitive to the snow grain size and shape, the small difference of albedo between case S and D indicates the difference of the optically characteristics on snow-grain size and shape between case S and D. However, the albedo of case S and D are considered to be almost same because the difference of the grain size corresponding to each albedo is small in case of the small grain. Therefore, the optically-equivalent snow grain sizes of case S and D were analogous. We compared the theoretically calculated albedos with observed ones to examine the optically properties of these two different types of snow.

B. Comparison between the theoretically calculated albedo and the observed one

1. Spherical particles (Case S)

The observed spectral albedo for case S and the theoretically calculated ones for three kinds of snow grains (r_{eff} = 10, 20, and 50 μm) are presented in Fig. 6. The spectral albedos were calculated using a two-snow-layer model, in which the model calculation parameters for the first layer were set to d_s = 5 cm and ρ_s = 0.155 g/cm^3, and those for the second layer were set to d_s = 26 cm and $\overline{\rho}_s$ = 0.276 g/cm^3, where $\overline{\rho}_s$ is the mean value in the second layer. These were determined from the snow pit work (Fig. 4a). The snow grain radius in Fig. 6, for which the theoretical albedo agreed with the observed albedo, was estimated to be just less than r_{eff} = 20 μm. This value was consistent with the measured snow grain size r_2 (10 to 30 μm) obtained in the snow pit work (Fig. 4a). Thus, the optically-equivalent snow grain size of the spherical snow particles was r_2, as indicated by Aoki *et al.*[14]

2. Dendrites (Case D)

We calculated the spectral albedos with the MC-RTM using a model of the non-spherical

ice particles to clarify the optical properties of dendrites. A model with hexagonal ice particles instead of spherical ones is known to be useful when comparing non-spherical ice particles with the observed albedos of various snow types in the Alps.[43] We here examined our crystal shapes in Fig. 3b, in which a portion of the tips of branches in the dendrites resemble hexagonal plates, but few of the branches have a regular structure because an edge of snow crystals rounds by sublimation after snowfall. We simply assumed the randomly-oriented circular cylindrical ice particles for dendrites to be non-spherical particles to simulate the characteristics of long and narrow branches of dendrites in this study. The single scattering properties of the circular cylindrical ice particles were calculated by the ray-tracing technique.[28]

Micrographs were used to estimate the lengths of circular cylinder along with the image-processing software "Image Hyper Pro" (Inter Quest Inc., Japan) to determine the size of the non-spherical ice particles. Digitized images of micrographs of snow grains were converted to binary tones with an appropriate threshold level. Highly aggregated grains were masked and excluded from the analysis. Each snow grain was defined by dividing the branches at the base of the branch from the other parts. We directly measured the radius R ($2R$ indicates the branch width) and the length L for these separated snow grains. The result of this analysis is presented in Table 1, where the mean values of R and L are 14.2 μm, and 189.3 μm. The spectral albedos were calculated based on this result using a two-snow-layer model, in which the first layer consisted of circular cylindrical ice particles with d_s = 31.5 cm and $\overline{\rho}_s$ = 0.033 g/cm^3, where $\overline{\rho}_s$ is the mean value of the first layer, and the second layer consisted of spherical ice particles with d_s = 25.5 cm and ρ_s = 0.272 g/cm^3. These parameters of d_s and ρ_s are the observed values obtained by snow pit work (Fig. 4b). We used five sizes and shapes for the circular cylinders in the spectral albedo calculation, as indicated in Table 2.

Figure 7 shows the theoretically calculated albedo using circular cylinders and the measured albedo for case D. The snow albedo is influenced by both dimensions R and L of circular cylinders. The shape of the snow grain affects not only the snow albedo but also snow reflectance.[44] The measured spectral albedo could be successfully simulated by any of (i) to (v) at visible wavelengths, but the albedos (i) and (iv) were overestimated at near-infrared wavelengths, and albedo (v) was somewhat underestimated for λ = 1.5 to 2.2 μm. The best-fitted cases were (ii) and (iii), where R = 14 μm and L was 190 μm and 380 μm. The value of R = 14 μm was the same as the measured branch width (14.2 μm) from the image processing, and the values of L were the same as or longer than the measured branch length (189.3 μm). This suggests that the snow albedo for dendrites in the near-infrared region essentially depends on the branch width, provided in Table 1, and the branch length must be sufficiently long ($L >> R$). The value of R = 14 μm falls in the measured range of r_2 (10 to 30 μm) observed from the snow pit work (Fig. 4b); therefore, dimension R of a circular cylinder with a sufficiently long L is the optically equivalent snow grain size for dendrites.

3. Relationship of optical properties between case S and case D

It is very convenient if the spectral albedo of snow composed of non-spherical ice particles can be simulated by the spherical ice particle model, because non-spherical particles generally have several dimensions that define their shape and size, while spherical particles have only one dimension. Grenfell and Warren[24] demonstrated that the scattering and absorption properties of a non-spherical ice particle can be represented using an equal volume-area ratio (V/A) sphere from theoretical calculations for a randomly oriented, infinitely long circular cylinder of ice, taking into account number concentration of the circular cylinder of ice. Although this approach is

normally valid for the flux computation, it may introduce substantial errors in the computation of the radiances.[24] We estimated the radius of an equal-V/A sphere by assuming our snow grains to be circular cylinders. The radius of the equal-V/A sphere r_{VA} for a circular cylinder is given by

$$r_{VA} = \frac{3RL}{2(R+L)}. \quad (1)$$

The best-fit case of the theoretically calculated albedos with the measured ones were (ii) and (iii), where $r_{VA} \sim 20$ μm (Table 2), as described in the previous section for case D. This value is close to the optically equivalent snow grain size (14 μm) and falls within the range of the branch width r_2 (10 to 30 μm) measured in the snow pit work (Fig. 4b).

The observed albedo for case S was almost the same as that for case D, as indicated in Fig. 5. The observed albedo for case S agreed with the theoretically calculated albedo, with the MC-RTM for r_{eff} being just less than 20 μm. This value agrees well with $r_{VA} \sim 20$ μm for case D. This indicates that the spectral albedo for the snow of dendrites can be represented by the radius of an equal-V/A sphere of a circular cylinder size, which supports the results of Grenfell and Warren.[24]

5. Summary and Conclusions

The optical properties of the artificial snowpacks with spherical (case S) and non-spherical (case D) particles were examined by the observed spectral albedos and Monte Carlo radiative transfer model of snow. Since our measurement was made at the cold laboratory, the influences of the instrument setup of the cold laboratory on the spectral albedo were examined, described in Appendix A. For case S, we examined the effect of the cluster of the spheres on the snow albedo using a generalized multiparticle Mie-solution model[33, 34] because snow grains are a little aggregate. The snow albedo of cluster of the spheres can be represented with that of the singe sphere slightly larger than its component of the cluster in case of small grains.

The theoretically calculated albedo for case S was consistent with the observed one for the same snow grain size. The optically equivalent snow grain size of the spherical particles was related to r_2. For case D, the snow albedos for the non-spherical particles are generally found to be influenced by the branch width and the branch length. A comparison of the estimated snow grain size by MC-RTM with the observed one from the snow pit work indicated that the optically equivalent snow grain radius of the dendrites may be related to the branch width of the dendrites.

Since the observed spectral albedo for case S was almost the same as that for case D at wavelengths of $\lambda = 0.35$ to 2.5 μm, the relationship of the optical properties between the two types of snowpack was examined to simulate the spectral snow albedo with non-spherical particles using the spherical ice particle model. The snow grain size of the spherical particles estimated by MC-RTM was just 20 μm. The radius of the equal-V/A sphere for non-spherical particles (dendrite) was also 18 - 20 μm, assuming the snow particles to be circular cylinders. These values agree well with the measured grain size for r_2. The relationship of the optical properties for spherical and non-spherical snow particles revealed that the equal-volume/area sphere represents the spectral albedos of the non-spherical particles. This treatment is very convenient for simulating the snow albedo in a climate model and retrieving the snow grain size from remote sensing data.

Appendix A. Effects of instrument setup on snow albedo

The effects of the instrument setup on snow albedo are potentially significant for changing the spectral albedo in a cold laboratory. We must consider these effects, which included the snow area being finite and some photons escaping from the snow wall (Fig. 1c), the area of light source being finite, nonparallel emitted light, and the shadow of the WRS that was present over the snow surface. We examined these effects of the instrument setup on the snow albedo using the Monte Carlo radiative transfer model (MC-RTM) and doubling and adding radiative transfer model (DA-RTM).

1. Effects of a finite snowfield and snow wall on snow albedo

The effect of a finite snow area on the snow albedo was firstly examined for case S by MC-RTM and DA-RTM for an infinite snow area. For this purpose, we compared the simulated albedo under the assumptions that the snow wall was completely covered by the snow container (hereafter, MC-RTM1) and the snowfield was infinite. Figure A1 shows the albedos simulated by MC-RTM1 and DA-RTM. The snow albedos calculated by MC-RTM1 were lower than those by DA-RTM at all wavelengths. This indicates that a finite snowfield causes a snow albedo reduction under the assumed conditions of the instrument setup.

The effects of the snow wall on the snow albedo were examined next. The spectral albedos calculated by MC-RTM under real observation conditions, in which the snow wall is not completely covered by the snow container, as illustrated in Fig. 1 and Fig. 4a, are also provided in Fig. A1 (hereafter, MC-RTM2). The difference in albedos between MC-RTM1 and MC-RTM2 indicates the effects of the metal wall height. The spectral albedos calculated by the MC-RTM2 were lower than those by MC-RTM1 at all wavelengths, since a portion of the light penetrating into the snow escapes from the snow wall at the sides of the snow container. The snow wall of the snow container also functions to reduce the albedo at all wavelengths. As a result, the theoretical albedo determined by MC-RTM is consistent with the observed one, taking into account the effects of the instrument setup.

2. Effects of a finite light source and height of the WRS on the snow albedo

The effects of a finite light source and the height of the WRS on the snow albedo were examined for case S. The spectral albedos were simulated as a function of the height of the WRS h (Fig. A2). The spectral albedos were the highest for all the wavelengths for h = 12 to 15 cm, which is expressed as h_M. The spectral albedos increased with the WRS height of $h < h_M$. This is primarily due to the effect of the WRS's shadow on the snow surface, which is significant (minimal) for a lower (higher) WRS position. The snow albedo decreased gradually when $h > h_M$. This can be explained by the relationships of the WRS with the finite snowfield and light source. The WRS came close to the light source and moved away from the snow surface as the WRS height increased. This resulted in (1) the shadow effect of the WRS decreasing relatively; (2) the downward flux received by the WRS increasing as the WRS approached the lamps, and (3) the measured upward flux decreasing because the field of view of the snow surface from under the surface of the WRS narrowed. Effect (1) increased the snow albedo and effects (2) and (3) decreased it. The effects of (2) and (3) on the snow albedo were greater than that of (1) since the effects (2) and (3) contributed to a decreasing albedo for a WRS height of $h > h_M$. Therefore, the spectral albedo depends on the height of the WRS in conjunction with the light source areas and snow surface at all wavelengths.

This work was conducted as cooperative research with the Meteorological Research

Institute, Japan, and the National Research Institute for Earth Science and Disaster Prevention, Japan. This study was supported in part by ADEOS-II/GLI Cal/Val experiments, supported by the Japan Aerospace Exploration Agency, and in part by the Research Fellowships of the Japan Society for the Promotion of Science for Young Scientists. We would like to thank N. Matsuoka, R. Anma, and H. Ishimoto for their many discussions and T. Takeda for operating the laboratory equipment of the cold laboratory.

References

1. Intergovernmental Panel for Climate Change (IPCC), *Climate change 2001: The scientific basis: Contribution of working group I to the third assessment report of the international panel on climate change* (Cambridge Univ. Press, New York, 2001).
2. P. Ya. Groisman, T. R. Karl and R. W. Knight, "Observed impact of snow cover on the heat balance and the rise of continental spring temperatures," Science. **263**, 198 – 200 (1994).
3. S. G. Warren, "Optical properties of snow," Rev. Geophys. and Space Phys. **20**, 67 – 89 (1982).
4. Te. Aoki, A. Hachikubo and M. Hori, "Effects of snow physical parameters on shortwave broadband albedos," J. Geophys. Res. **108**, doi:10.1029/2003JD003506 (2003).
5. J. Hansen and L. Nazarenko, "Soot climate forcing via snow and ice albedos," Proc. Natl. Acad. Sci. USA., **101**, 423 – 428 (2004).
6. H. Motoyoshi, Te. Aoki, M. Hori, O. Abe and S. Mochizuki, "Possible effect of anthropogenic aerosol deposition on snow albedo reduction at Shinjo, Japan," J. Meteor. Soc. Japan. **83A**, 137 – 148 (2005).
7. T. P. Barnett, L. Dümenil, U. Schlese, E. Roeckner and M. Latif, "The effect of Eurasian snow cover on regional and global climate variations," J. Atmos. Sci. **46**, 661 – 685 (1989).
8. G. H. Liljequist, "Energy exchange of an Antarctic snow field: Short-wave radiation (Maudheim 71°03'S, 10°56'W), in Norwegian-British-Swedish Anterctic Expedition, 1949 – 52, Scientific Results," vol. 2, part 1A, Norsk Polarinstitutt, Oslo, (1956).
9. T. C. Grenfell and G. A. Maykut, "The optical properties of ice and snow in the Arctic basin," J. Glaciol. **18**, 445 – 463 (1977).
10. M. Kuhn and L. Siogas, "Spectroscopic studies at McMurdo, South Pole, and Siple Stations during the austral summer 1977-78," Antarct. J. U. S. **13**, 178 – 179 (1978).
11. T. C. Grenfell, "A visible and near-infrared scanning photometer for field measurements of spectral albedo and irradiance under polar conditions," J. Glaciol. **27**, 476 – 481 (1981).
12. T. C. Grenfell, D. K. Perovich and J. A. Ogren, "Spectral albedos of an alpine snowpack," Cold Reg. Sci. Technol. **4**, 121 – 127 (1981).
13. Te. Aoki, Ta. Aoki, M. Fukabori, Y. Tachibana, Y. Zaizen, F. Nishio and T. Oishi, "Spectral albedo observation on the snow field at Barrow, Alaska," Polar Meteorol. Glaciol. **12**, 1 - 9 (1998).
14. Te. Aoki, Ta. Aoki, M. Fukabori, A. Hachikubo, Y. Tachibana, and F. Nishio, "Effects of snow physical parameters on spectral albedo and bi-directional reflectance of snow surface," J. Geophys. Res. **105**, 10,219 – 10,236 (2000).
15. T. Nakamura, O. Abe, T. Hasegawa, R. Tamura, and T. Ohta, "Spectral reflectance of snow with a known grain-size distribution in successive metamorphism," Cold Reg. Sci. Technol. **32**, 13 - 26 (2001).
16. W. J. Wiscombe and S. G. Warren, "A model for the spectral albedo of snow, I, Pure snow," J. Atmos. Sci. **37**, 2712 – 2733 (1980).
17. S. G. Warren and W. J. Wiscombe, "A model for the spectral albedo of snow, II, Snow containing atmospheric aerosols," J. Atmos. Sci. **37**, 2734 – 2745 (1980).
18. P. Chýlek, V. Ramaswamy and V. Srivastava, "Albedo of soot-contaminated snow," J. Geophys. Res. **88**, 10,837 – 10,843 (1983).
19. B. Bourdelles and M. Fily, "Snow grain-size determination from Landsat imagery over Terre Adélie, Antarctica," Ann. Glaciol. **17**, 86 - 92 (1993).
20. A. W. Nolin and J. Dozier, "A hyperspectral method for remotely sensing the grain size of snow," Remote Sens. Environ. 74, 207 – 216 (2000).

21. M. Fily, B. Bourdelles, J. P. Dedieu and C. Sergent, “Comparison of In Situ and Landsat Thematic Mapper derived snow grain characteristics in the Alps,” Remote Sens. Environ. **59**, 452 – 460 (1997).
22. T. H. Painter, D. A. Roberts, R. O. Green and J. Dozier, “The effect of grain size on spectral mixture analysis of snow-covered area from AVIRIS data,” Remote Sens. Environ. **65**, 320 – 332 (1998).
23. T. Tanikawa, Te. Aoki, and F. Nishio, “Remote sensing of snow grain size and snow impurities from Airborne Multispectral Scanner data using a snow bidirectional reflectance distribution function model,” Ann. Glaciol. **34**, 74 – 80 (2002).
24. T. C. Grenfell and S. G. Warren, “Relationship of a nonspherical ice particle by a collection of independent sphere for scattering and absorption of radiation,” J. Geophys. Res. **104**, 31,697 – 31,709 (1999).
25. M. I. Mishchenko, J. W. Hovenier and L. D. Travis, *Light Scattering by Nonspherical Particles* (Academic Press, California, 2000).
26. A. A. Kokhanovsky and E. P. Zege, “Scattering optics of snow,” Appl. Opt., **43**, 1,589 – 1,602 (2004).
27. G. I. Marchuk, G. A. Mikhailov, M. A. Nazaraliev, R. A. Darbinjan, B. A. Kargin and B. S. Elepov, *The Monte Carlo Methods in Atmospheric Optics* (Springer, New York, 1980).
28. A. Macke and M. I. Mishchenko, “Applicability of regular particles shapes in light scattering calculations for atmospheric ice particles,” Appl. Opt. **35**, 4291 - 4296 (1996).
29. T. C. Grenfell, S. G. Warren and P. C. Mullen, “Reflection of solar radiation by the Antarctic snow surface at ultraviolet, visible, and near-infrared wavelengths,” J. Geophys. Res. **99**, 18,669 – 18,684 (1994).
30. C. Sergent, C. Leroux, E. Pougatch, and F. Guirado, “Hemispherical-directional reflectance measurements of natural snow in the 0.9 – 1.45 μm spectral range: comparison with adding-doubling modeling,” Ann. Glaciol. 26, 59 – 63 (1998).
31. M. I. Mishchenko, “Asymmetry parameters of the phase function for densely packed scattering grains,” J. Quant. Spectrosc. Radiat. Transfer. **52**, 95 – 110 (1994).
32. M. I. Mishchenko and A. Macke, “Asymmetry parameters of the phase function for isolated and densely packed spherical particles with multiple internal inclusions in the geometric optics limit,” J. Quant. Spectrosc. Radiat. Transfer. 57, 767 – 794 (1997).
33. A. A. Kokhanovsky, *Optics of light scattering media: Problems and Solutions*, (John Wiley & Sons, Chichester, U.K., 1998)
34. Y.-l. Xu, “Electromagnetic scattering by an aggregate of spheres,” Appl. Opt. **34**, 4573 – 4588 (1995).
35. Y.-l. Xu and N. Khlebtsov, “Orientation-averaged radiative properties of an arbitrary configuration of scatterers, ” J. Quant. Spectrosc. Radiat. Transfer. **79-80**, 1121-1137 (2003).
36. P. Yang and K. N. Liou, “Single-scattering properties of complex ice crystals in terrestrial atmosphere,” Contr. Atmos. Phys. 71, 223 – 248 (1998)
37. M. I. Mishchenko, D. W. Mackowski, and L. D. Travis, "Scattering of light by bispheres with touching and separated components," Appl. Opt. **34**, 4589 – 4599 (1995).
38. S. G. Warren, “Optical constants of ice from the ultraviolet to microwave,” Appl. Opt. **23**, 1206 – 1225 (1984).
39. L. Kou, D. Labrie, and P. Chýlek, “Refractive indices of water and ice in the 0.65- to 2.5 μm spectral range,” Appl. Opt. **32**, 3531 – 3540 (1993).

40. M. Sydor, J. A. Sorensen and V. Shuter, “Remote sensing of snow albedo for determination of dustfall,” Appl. Opt. **18**, 3574 – 3578 (1979).
41. M. Fily, B. Bourdelles, J. –P. Dedieu and C. Sergent, “Comparison of in situ and Landsat thematic mapper derived snow grain characteristics in the Alps,” Remote Sens. Environ., **59**, 452 – 460 (1997).
42. M. Hori, Te. Aoki, K. Stamnes, B. Chen and W. Li, “Preliminary validation of the GLI cryosphere algorithms with MODIS daytime data,” Polar Meteorol. Glaciol. **15**, 1 – 20 (2001).
43. C. Leroux, J. Deuzé, P. Goloub, C. Sergent, and M. Fily, “Ground measurements of the polarized bidirectional reflectance of snow in the near-infrared spectrum domain: Comparisons with model results,” J. Geophys. Res. **103**, 19,721 – 19,731 (1998).
44. M. I. Mishchenko, J. M. Dlugach, E. G. Yanovotskij and N. T. Zakharova, "Bidirectional reflectance of flat, optically thick particulate layers: an efficient radiative transfer solution and applications to snow and soil surfaces," J. Quant. Spectrosc. Radiat. Transfer. **63**, 409 – 432 (1999).

Table 1. Results of micrograph measurements of the dendrites. R is the half-width of the base and L is the length of a circular cylinder.

	R (μm)	L (μm)
Average (Max. – Min.)	14.2 (25.4 - 6.4)	189.3 (828.8 – 36.1)
Standard deviation	4.2	137.2

Table 2. Radius of the equal-V/A sphere r_{VA} determined by assuming the snow grains to be circular cylinders. R is the half-width of the base and L is the length of the circular cylinder.

Circular cylinder (μm)	r_{VA} (μm)
(i) $R = 14$, $L = 95$	18.3
(ii) $R = 14$, $L = 190$	19.6
(iii) $R = 14$, $L = 380$	20.3
(iv) $R = 7$, $L = 190$	10.1
(v) $R = 28$, $L = 190$	36.6

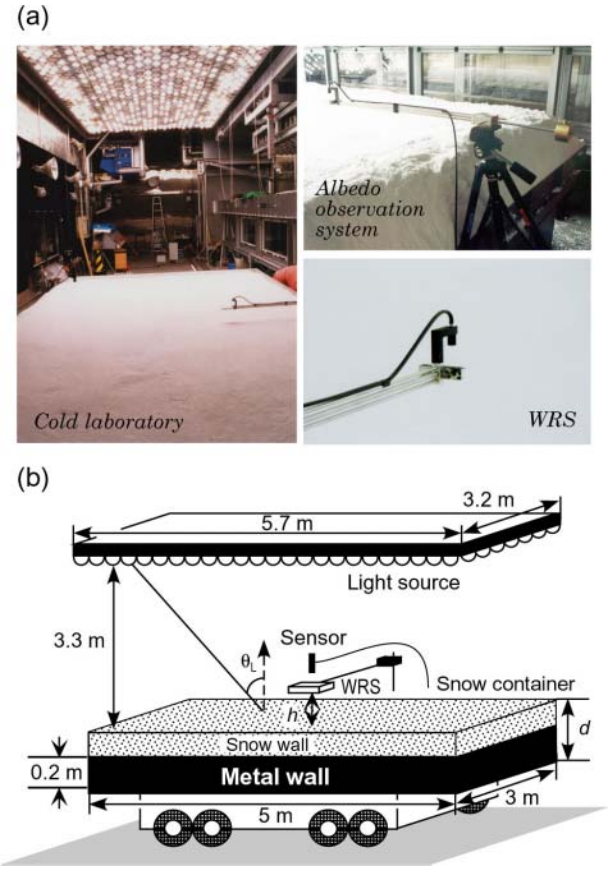

Figure 1. (a) Photographs of the cold laboratory, albedo observation system, and white reference standard (WRS). (b) Schematic illustration of the instrument setup for the snow container and light source in the cold laboratory. The snow was produced by an artificial snowfall system, which was set beneath the ceiling of the cold laboratory. The snow lies on a 3 m × 5 m snow container with a metal wall 0.2 m high. The light source moves above the snow container when the optical measurement is made. Parameters are snow depth d and height h of white reference standard (WRS) above the snow surface. The WRS (6 × 6 cm) is placed at h = 10 cm above the snow surface and positioned 1 m from the side of the snow container.

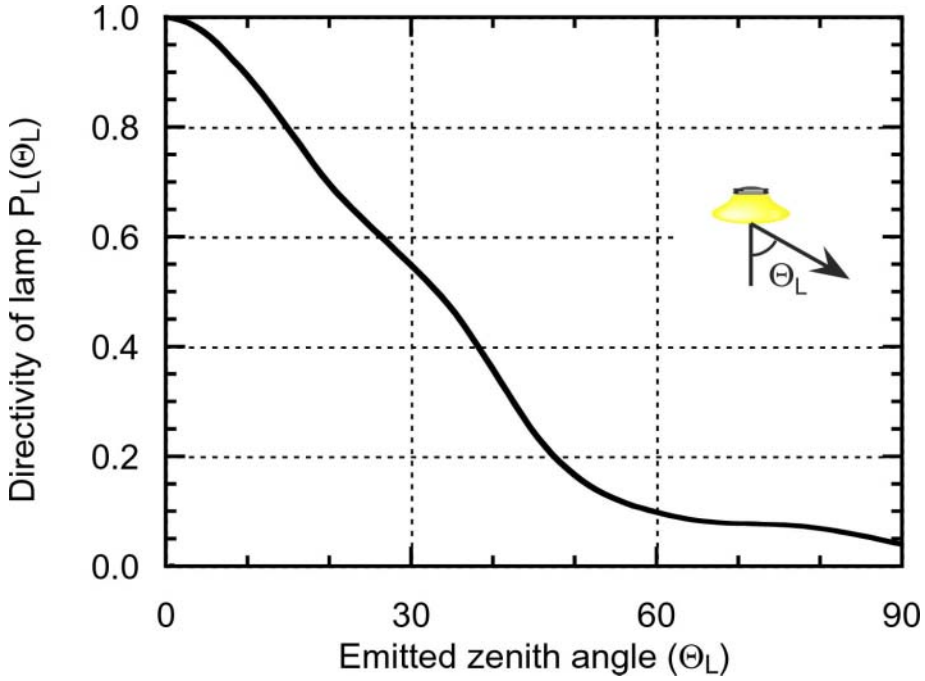

Figure 2. Directivity of the light intensity emitted from a lamp as a function of the emitted zenith angle Θ_L, which is normalized by the intensity at the nadir ($\Theta_L = 0°$). There is almost no spectral dependence of directivity.

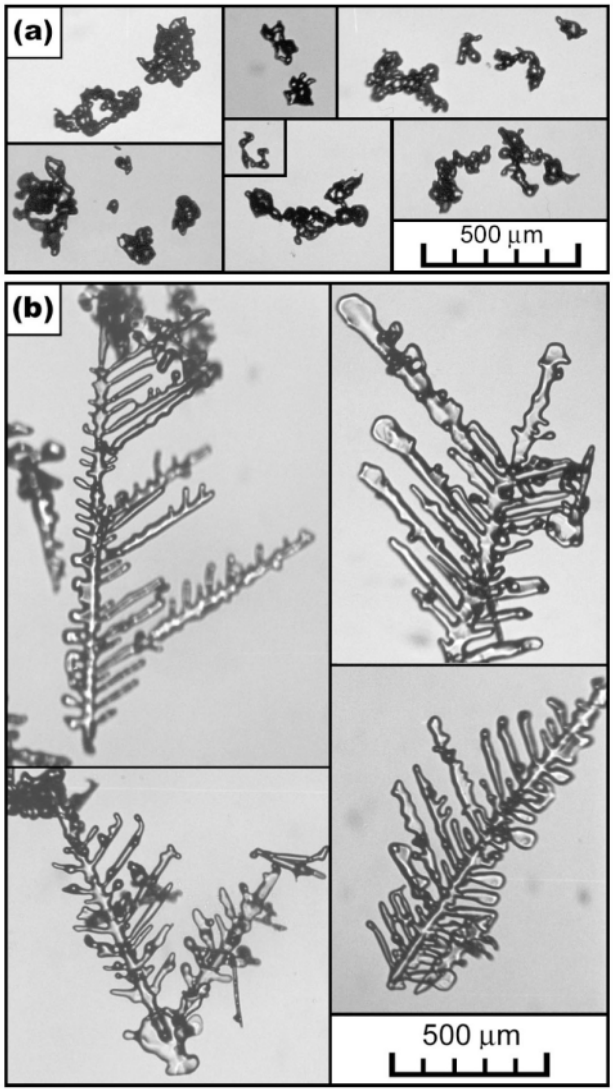

Figure 3. Micrographs of artificial snow crystals; (a) spherical particles (case S), and (b) dendrites (case D).

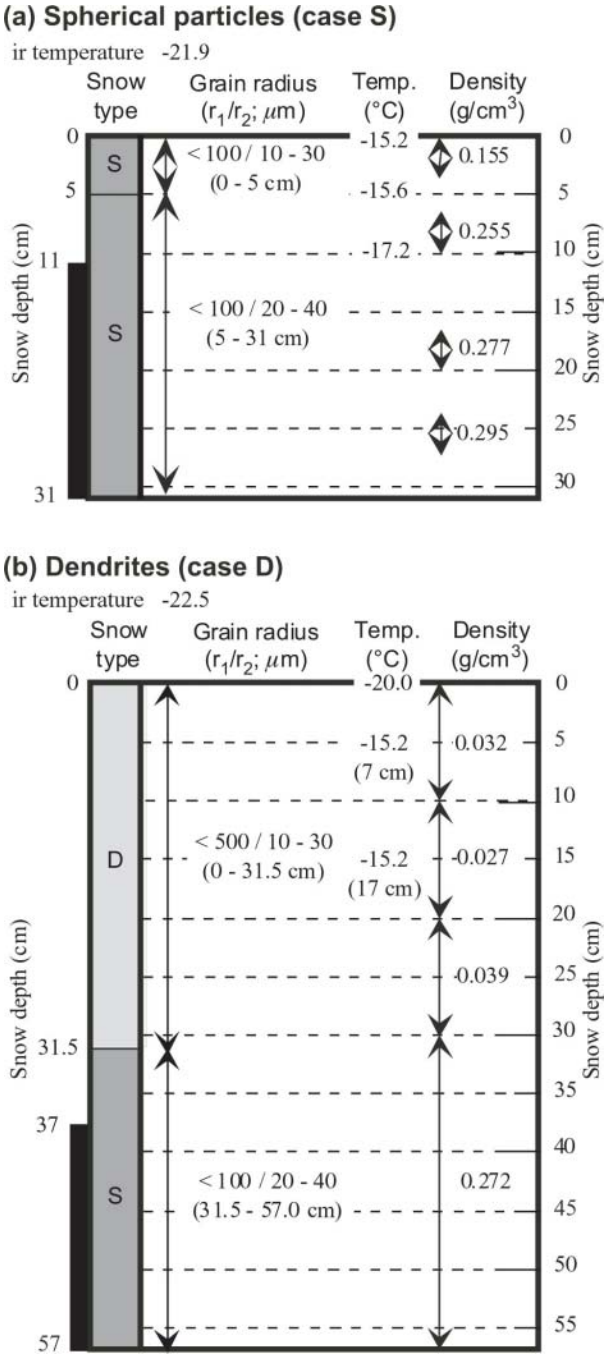

Figure 4. Vertical profiles of snow parameters observed during snow pit work for (a) spherical particles (case S), and (b) dendrites (case D). S and D in snow type mean spherical particles and dendrites, respectively. The snow grain size was measured at a 10 μm resolution using a handheld lens. There were two grain size dimensions: one-half the length of the major axis of the dendrites or cluster of aggregated spherical grains (r_1), and one-half the branch width of the dendrites or each spherical particle (r_2). The lower part, designated by a black bar of snow layers from the bottom to 20 cm, was enclosed by a metal wall, while the upper part was exposed.

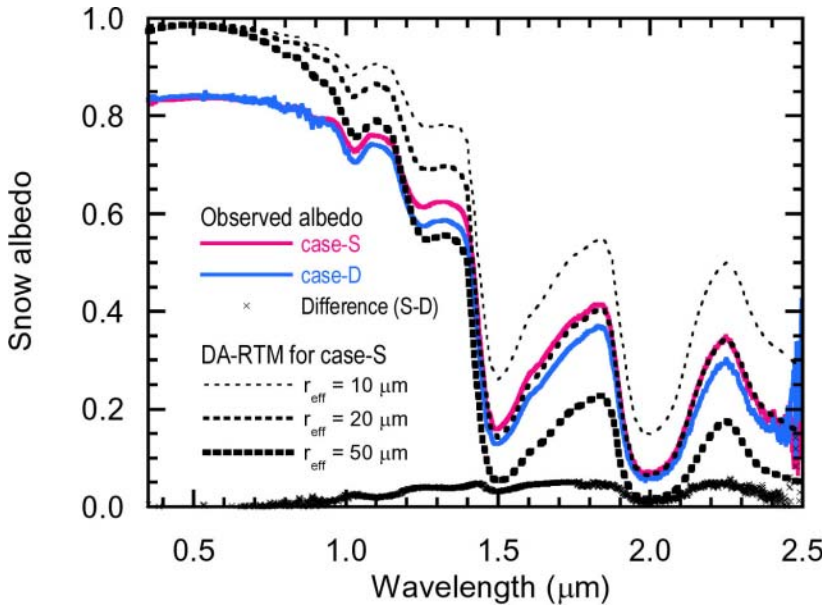

Figure 5. Observed spectral albedos for spherical particles (case S) and dendrites (case D), difference of spectral albedos for case S and D, and theoretically calculated albedos using DA-RTM for case S (r_{eff} = 10, 20, and 50 μm). The observed spectral albedos were obtained by averaging five spectral albedos calculated from five pairs of measurements for downward and upward fluxes.

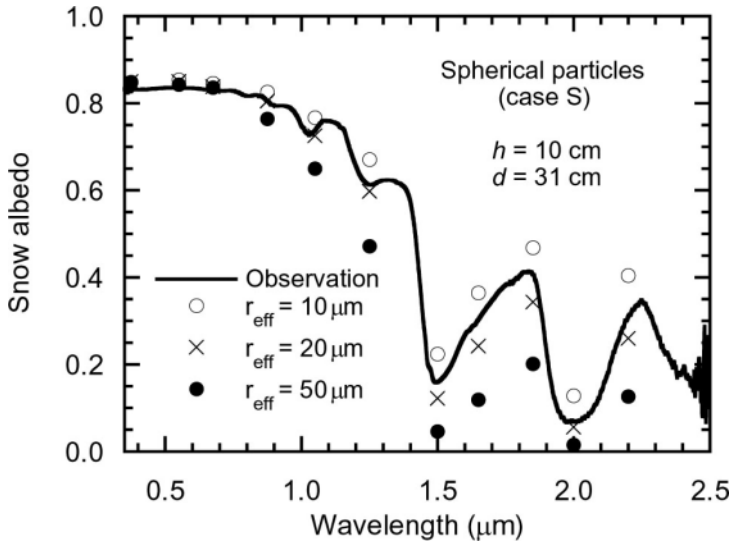

Figure 6. Comparison between the observed spectral albedos for spherical particles (case S) and theoretically calculated albedos using MC-RTM for spherical particles with r_{eff} = 10, 20, and 50 μm. The latter were calculated with a two-snow-layer model (first layer surface to 5 cm; second layer 5 to 31 cm), under the same conditions as those in Fig. 1.

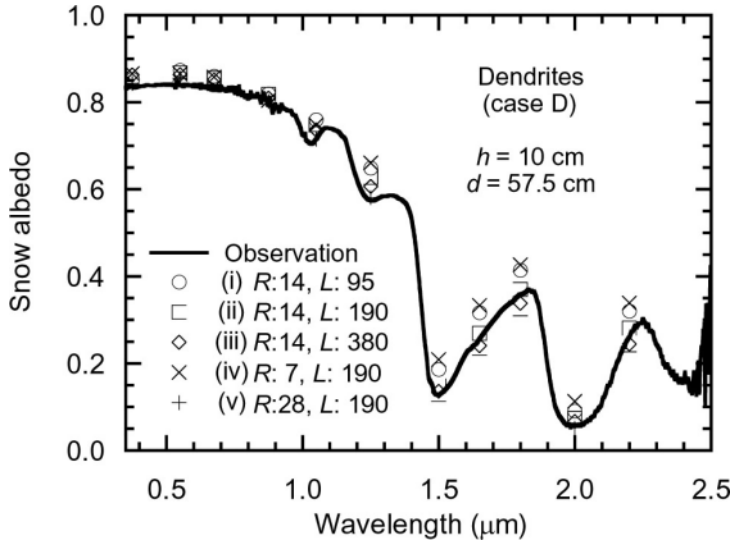

Figure 7. Comparison between measured spectral albedos for dendrites (case D) and theoretically calculated albedos using MC-RTM for the five kinds of cylindrical ice particles (unit: μm) listed in Table 2. The latter were calculated with a two-snow-layer model (first layer surface to 31.5 cm; second layer 31.5 to 57 cm), under the same conditions as those in Fig. 1.

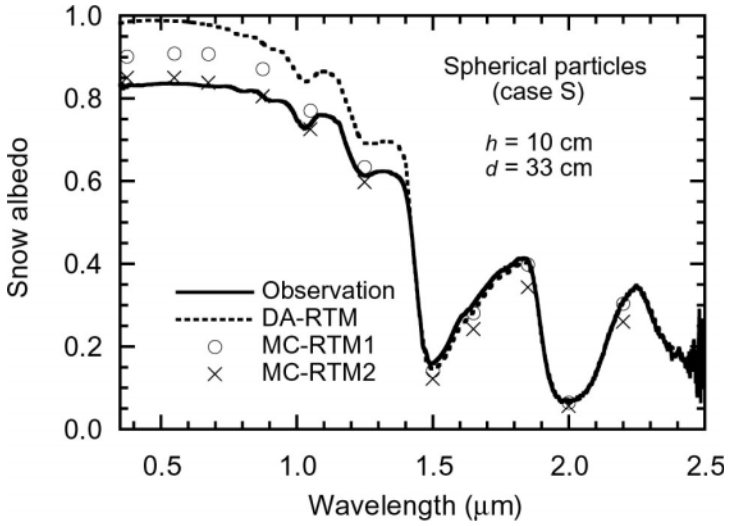

Figure A1. Comparison of theoretically calculated albedos using DA-RTM and MC-RTM for r_{eff} = 20 μm (case S). The observed albedos are also provided for reference. The circle in this figure indicates the calculated albedo under the assumption that the snow wall is completely covered by a metal wall (MC-RTM1), and the cross indicates the assumption of real instrument conditions, under which the snow wall is not completely covered by the snow container (MC-RTM2), as described in Fig. 1.

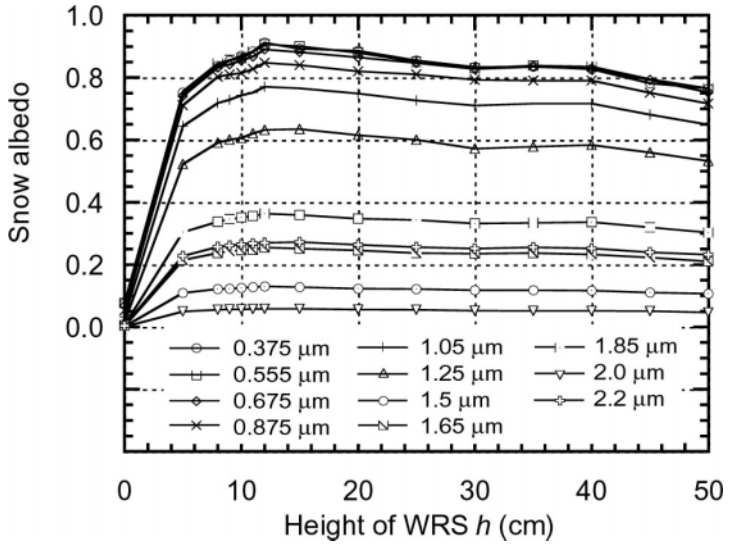

Figure A2. Theoretically calculated albedos using MC-RTM as a function of the WRS's height h for the snow with spherical particles of r_{eff} = 20 μm.

Table and Figure caption

Table 1. Results of micrograph measurements of the dendrites. R is the half-width of the base and L is the length of a circular cylinder.

Table 2. Radius of the equal-V/A sphere r_{VA} determined by assuming the snow grains to be circular cylinders. R is the half-width of the base and L is the length of the circular cylinder.

Figure 1. (a) Photographs of the cold laboratory, albedo observation system, and white reference standard (WRS). (b) Schematic illustration of the instrument setup for the snow container and light source in the cold laboratory. The snow was produced by an artificial snowfall system, which was set beneath the ceiling of the cold laboratory. The snow lies on a 3 m × 5 m snow container with a metal wall 0.2 m high. The light source moves above the snow container when the optical measurement is made. Parameters are snow depth d and height h of white reference standard (WRS) above the snow surface. The WRS (6 × 6 cm) is placed at h = 10 cm above the snow surface and positioned 1 m from the side of the snow container.

Figure 2. Directivity of the light intensity emitted from a lamp as a function of the emitted zenith angle Θ_L, which is normalized by the intensity at the nadir ($\Theta_L = 0°$). There is almost no spectral dependence of directivity.

Figure 3. Micrographs of artificial snow crystals; (a) spherical particles (case S), and (b) dendrites (case D).

Figure 4. Vertical profiles of snow parameters observed during snow pit work for (a) spherical particles (case S), and (b) dendrites (case D). S and D in snow type mean spherical particles and dendrites, respectively. The snow grain size was measured at a 10 μm resolution using a handheld lens. There were two grain size dimensions: one-half the length of the major axis of the dendrites or cluster of aggregated spherical grains (r_1), and one-half the branch width of the dendrites or each spherical particle (r_2). The lower part, designated by a black bar of snow layers from the bottom to 20 cm, was enclosed by a metal wall, while the upper part was exposed.

Figure 5. Observed spectral albedos for spherical particles (case S) and dendrites (case D), difference of spectral albedos for case S and D, and theoretically calculated albedos using DA-RTM for case S (r_{eff} = 10, 20, and 50 μm). The observed spectral albedos were obtained by averaging five spectral albedos calculated from five pairs of measurements for downward and upward fluxes.

Figure 6. Comparison between the observed spectral albedos for spherical particles (case S) and theoretically calculated albedos using MC-RTM for spherical particles with r_{eff} = 10, 20, and 50 μm. The latter were calculated with a two-snow-layer model (first layer surface to 5 cm; second layer 5 to 31 cm), under the same conditions as those in Fig. 1.

Figure 7. Comparison between measured spectral albedos for dendrites (case D) and theoretically calculated albedos using MC-RTM for the five kinds of cylindrical ice particles (unit: μm) listed in Table 2. The latter were calculated with a two-snow-layer model (first layer surface to 31.5 cm; second layer 31.5 to 57 cm), under the same conditions as those in Fig. 1.

Figure A1. Comparison of theoretically calculated albedos using DA-RTM and MC-RTM for r_{eff} = 20 μm (case S). The observed albedos are also provided for reference. The circle in this figure indicates the calculated albedo under the assumption that the snow wall is completely covered by a metal wall (MC-RTM1), and the cross indicates the assumption of real instrument conditions, under which the snow wall is not completely covered by the snow container (MC-RTM2), as described in Fig. 1.

Figure A2. Theoretically calculated albedos using MC-RTM as a function of the WRS's height h for the snow with spherical particles of r_{eff} = 20 μm.